Quantum confined Rydberg excitons in Cu_2O nanoparticles

Konstantinos Orfanakis, Sai Kiran Rajendran, and Hamid Ohadi*
SUPA, School of Physics and Astronomy, University of St. Andrews, St. Andrews KY16 9SS, United Kingdom

Sylwia Zielińska-Raczyńska, Gerard Czajkowski, Karol Karpiński, and David Ziemkiewicz
UTP University of Science and Technology, 85-796 Bydgoszcz, Poland

(Received 5 June 2020; revised 7 June 2021; accepted 8 June 2021; published 21 June 2021)

The quantum confinement of Rydberg excitons is an important step towards exploiting their large nonlinearities for quantum applications. We observe Rydberg excitons in natural nanoparticles of Cu_2O. We resolve up to the principal quantum number $n = 12$ in a bulk Cu_2O crystal and up to $n = 6$ in nanoparticles extracted from the same crystal. The exciton transitions in nanoparticles are broadened and their oscillator strengths decrease as $\propto n^{-4}$ compared to those in the bulk (decreasing as $\propto n^{-3}$). We explain our results by including the effect of quantum confinement of exciton states in the nanoparticles. Our results provide an understanding of the physics of Cu_2O Rydberg excitons in confined dimensions.

DOI: 10.1103/PhysRevB.103.245426

I. INTRODUCTION

Solid-state quantum systems provide unprecedented capabilities for the realization of novel devices owing to their robustness, miniaturization capability, and scalability [1–6]. The operation of such devices requires developing means to efficiently produce, control, and detect strongly interacting particles. Excitons, elementary excitations in semiconductors consisting of a Coulomb-bound pair of an electron and a hole, are considered major candidates towards this direction. An exciton represents a solid-state analog of the hydrogen atom and hence excited states can be observed as a hydrogen-like discrete series at energies R_y/n^2 below the band gap, with R_y the Rydberg energy and n the principal quantum number [7]. Excitons in cuprous oxide (Cu_2O) were observed as early as 1952 [8], and their various physical properties have been studied since then [9]. However, only energy levels up to $n = 8$ in Cu_2O were observed for many decades until the Rydberg spectrum was extended to $n = 12$ in 1996 [10].

Among semiconductors, Cu_2O has the advantage of a large Rydberg energy which allows access to much higher excited states. In a recent high-resolution laser absorption study [11], it was shown that Cu_2O hosts Rydberg excitons up to $n = 25$. This demonstration opened the portal to the field of giant Rydberg excitons in a solid state [12–20], in close analogy with their highly excited counterparts in atomic physics [21]. Owing to their giant microscopic dimensions (up to $\sim 1\,\mu$m) leading to the onset of the exciton blockade, Rydberg excitons in Cu_2O exhibit enhanced optical nonlinearities at much smaller densities compared with other traditional semiconductors [11,22]. These nonlinearities can be harnessed by quantum confinement of the excitons in semiconductor low-dimensional structures such as quantum wells and quantum dots [23]. Studying these excitons in confined dimensions is a crucial step towards harnessing these nonlinearities for applications [24,25]. Nanoparticles [26] are naturally a suitable system for quantum confinement and an interesting platform for realizing quantum technologies with Rydberg excitons, potentially underpinning future devices such as single-photon sources [27] and single-photon switches [28].

In this work, we report the observation of Rydberg excitons in nanoparticles of Cu_2O. We resolve the yellow p-exciton states in natural nanoparticles up to $n = 6$, while we observe up to $n = 12$ in the bulk crystal that the particles were extracted from. We show that the reduction of the crystal structure from bulk to nanoparticles leads to broadened linewidths and an apparent reduction of the oscillator strength of the excitonic peaks compared to that in the bulk. We describe both effects by the quantum confinement of the Rydberg states and the size distribution of our nanoparticles. Our results are the first demonstration of the effect of quantum confinement in linewidth and oscillator strength of Rydberg excitons.

II. EXPERIMENTAL METHODS

Cu_2O nanoparticles were extracted from the residual powder from polishing a natural crystal mined in Tsumeb, Namibia. After forming a suspension of Cu_2O powder in water, a droplet of this suspension is deposited onto a CaF_2 substrate. Scanning electron microscopy (SEM) reveals that Cu_2O particles tend to aggregate and form a thin layer due to Van der Waals forces as the particles redistribute during water evaporation [Fig. 1(a)]. The particles are of various sizes and shapes with a average and median diameter size of $\simeq$1.1 and $\simeq$0.7 nm [Fig. 1(b)]. We refer to these particles as natural nanoparticles (NNPs). Nanoparticles are compared to a thin slab of natural bulk crystal that is cut and mechanically polished down to a thickness of $\sim 60\,\mu$m.

*ho35@st-andrews.ac.uk

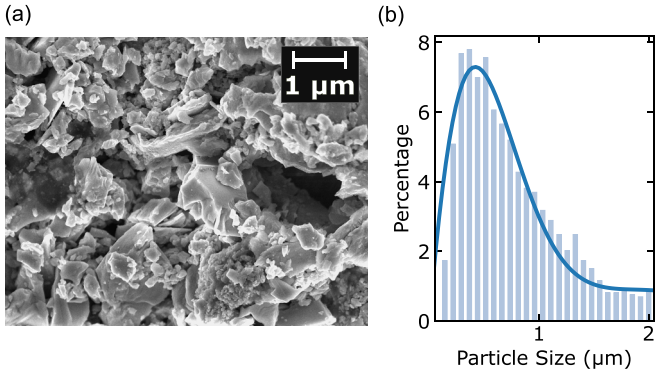

FIG. 1. (a) SEM image of a cluster of particles. (b) Particle size distribution. The fitted distribution is depicted as a blue solid line. The mean diameter is calculated as $\simeq$1.1 μm, while the median as $\simeq$0.7 μm.

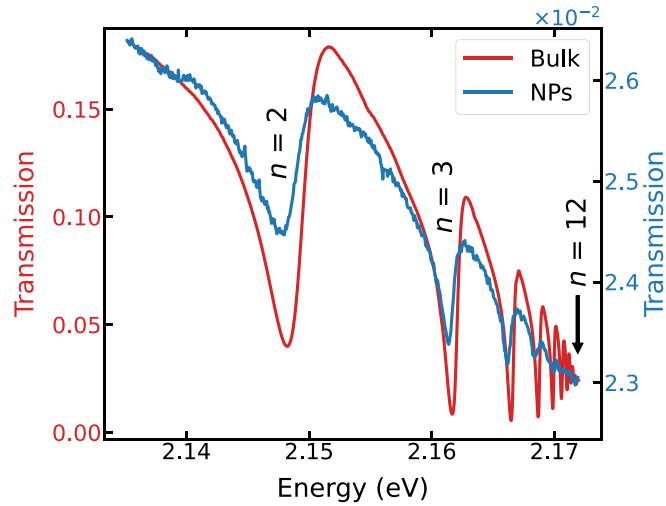

FIG. 2. Transmission spectrum for a natural crystal of Cu_2O at 4 K, where excitons up to $n = 12$ are resolved (red line) and for natural nanoparticles (blue line).

We perform broadband transmission spectroscopy [29]. The excitation source is a green-yellow light-emitting diode (LED) with a center wavelength of 554 μm (Thorlabs MINTF4). The resulting signal is collected, dispersed, and analyzed in a spectrometer (Andor Shamrock 750) coupled to a CCD camera. The spectrometer resolution at the yellow exciton transitions is 0.03 nm ($\sim$112 μeV). For transmission spectroscopy, an objective lens (20× Mitutoyo Plan Apo, NA = 0.42) focuses the excitation light to a spot on our sample ($\sim$100 μm diameter) and a second objective lens (same NA as excitation) collimates the transmitted light before it enters the spectrometer. The sample is maintained at 4 K using a liquid-helium flow cryostat. We use CaF_2 substrates because of their excellent thermal conductivity at cryogenic temperatures and transparency in the visible spectrum.

III. EXPERIMENTAL RESULTS

The transmission spectrum of the bulk crystal reveals a series of absorption lines corresponding to the excited states of Rydberg excitons in Cu_2O [red line in Fig. 2(b)]. These states are labeled by their principal quantum number, n. We can reliably identify Rydberg states up to $n = 12$ overlaid on a continuous phonon background [30,31]. The reduced number of exciton lines observed in our experiment compared to previous works [11] is primarily attributed to the small diameter and broadband spectrum of our excitation source. The asymmetric lineshape stems from the Fano interference between the discrete excitonic states and the absorption background originating from phonon-assisted absorption of the 1s exciton [32]. By fitting the exciton resonance energies to the Rydberg formula, we extract the band-gap energy $E_g = 2.173$ eV and the Rydberg energy $R_y = 97.1$ meV, which agree with those reported in the literature [10,33].

The transmission spectra of the nanoparticles covering a large area ($\sim$100 μm diameter) on the substrate show clear exciton peaks [blue line in Fig. 2(b)]. Exciton resonances are evident as discrete asymmetric dips on top of the phonon background. A noticeable difference between the spectra of clusters and that of the thinned bulk crystal is that, in the former, is the sharp decrease in the peak absorption of the excitons as n increase, such that we can only resolve resonances up to $n = 6$.

Repeating the measurements on synthetic nanoparticles (SNPs) of comparable sizes can show if the reduced number of observed excitonic resonances in NNPs could be due to the polishing procedure. The transmission spectrum for SNPs, exhibits the same number of resonances as the one for NNPs [34]. Therefore, we rule out polishing as the reason for the observation of the reduced number of transitions. We note that resonances with the same n are slightly blueshifted in the bulk crystal compared to those in nanoparticles due to a small temperature variation [35] in our experiment [36].

The comparison of oscillator strength (peak area) of the excitons in bulk and NPs shows [see Fig. 3(a)] that the relative peak area of excitons in nanoparticles of Cu_2O decreases as $\propto n^{-4}$ compared to that in the bulk (decreasing as $\propto n^{-3}$, which is the approximation of theoretical dependence for large n). Individual peaks were fitted with an asymmetric Lorentzian [11] [see also Eq. (6)] convoluted with a Gaussian function representing our spectrometer response function to extract their linewidth. The linewidth of NPs is approximately double the linewidth of the bulk thin crystal for the first three observed resonances. The broadening is more pronounced for $n = 5$ as the linewidth increases by nearly three folds for NPs [Fig. 3(b)].

Previously, the broadening of excitons in nanoparticles of CuCl (<15 nm diameter) was found to be due to quantum confinement and size distribution [37,38]. Here, we show that quantum confinement results in the broadening of the transitions in a similar process, however, due to the narrow linewidth of the transitions the effect is visible for larger nanoparticle sizes.

IV. THEORETICAL DESCRIPTION

From the point of view of the classification of low-dimensional semiconductor structures, the considered nanocrystals are quantum dots (QDs). The SEM images

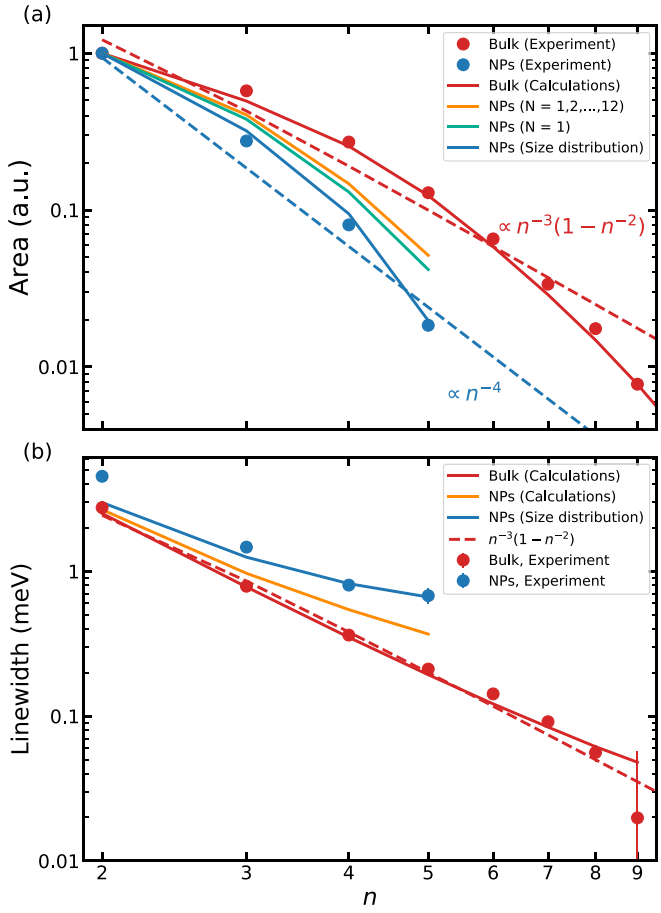

FIG. 3. (a) Peak areas and (b) linewidths calculated from experimental (dots) and theoretical results (lines). Peak areas are normalized to the value of $n = 2$ in each case.

(Fig. 1) suggest that the best model shape is a spherical quantum dot, with a median diameter of ∼700 nm. Assuming that the interaction between dots is small enough, we may consider interband transitions in an isolated QD, and then average the results over a size distribution of QDs. As it has been shown previously [39], the optical properties of QDs can be studied with the real density matrix approach (RDMA). In this method, the optical response (absorption, reflection, transmission) is obtained by solving a set of equations for the excitonic amplitude $Y(\mathbf{r}_e, \mathbf{r}_h, t)$ and electric field vector $\mathbf{E}(\mathbf{R}, t)$ of the wave propagating in the nanostructure. The quantities $\mathbf{r}_e, \mathbf{r}_h$ are the coordinates of the electron and the hole, and $\mathbf{R}$ is the center-of-mass coordinate of the electron-hole pair. The basic equations of RDMA have the form [39]

$$-i(\hbar\partial_t + \Gamma)Y(\mathbf{r}_e, \mathbf{r}_h, t) + H_{eh}Y(\mathbf{r}_e, \mathbf{r}_h) = \mathbf{ME}, \qquad (1)$$

where Γ is a phenomenological damping coefficient, $\mathbf{M}(\mathbf{r})$ is a smeared-out transition dipole density, E_g is the fundamental gap, and $\mathbf{r} = \mathbf{r}_e - \mathbf{r}_h$ is the relative electron-hole distance. The operator H_{eh} stands for the two-band effective mass Hamiltonian, which includes the electron and hole kinetic energy, the electron-hole interaction potential and the confinement potentials. In consequence, the Hamiltonian H_{eh} is given by

$$H_{eh} = E_g + \frac{\mathbf{p}_h^2}{2m_h} + \frac{\mathbf{p}_e^2}{2m_e} + V_{eh}(\mathbf{r}_e, \mathbf{r}_h) + V_h(\mathbf{r}_h) + V_e(\mathbf{r}_e), \qquad (2)$$

where the second and the third terms on the right-hand side (r.h.s.) are the electron and the hole kinetic energy operators with appropriate effective masses, the fourth term is the electron-hole attraction, and the two last terms are the surface confinement potentials for the electron and hole. The total polarization of the medium is related to the coherent amplitude by

$$\mathbf{P}(\mathbf{R}) = 2\mathrm{Re}\int d^3r\, \mathbf{M}(\mathbf{r})Y(\mathbf{R}, \mathbf{r}). \qquad (3)$$

This, in turn, is used in Maxwell's field equation

$$c^2\nabla^2\mathbf{E}(\mathbf{R}) - \epsilon_b\ddot{\mathbf{E}} = \frac{1}{\epsilon_0}\ddot{\mathbf{P}}(\mathbf{R}), \qquad (4)$$

where $\epsilon_b = 7.5$ is the QD material dielectric constant. Equations (1) to (4) form a system of coupled integro-differential equations in six-dimensional configuration space $(\mathbf{r}_e, \mathbf{r}_h)$ The optical properties of spherical QDs can be described by means of the exciton center-of-mass (COM) quantization method [39]. One assumes that the COM is confined within a sphere of radius $R_{\max}$, which will give the confinement states. Those states will overlap with the three-dimensional exciton states. The effective QD susceptibility in this limit is given by the formula [40]

$$\overline{\chi}_{\mathrm{QD}} = \epsilon_b \sum_{n=2}^{n_{\max}} \sum_{N=1}^{N_{\max}} \frac{f_{n1} f_N \Delta_{LT}^{(2)}/R_y}{(E_{Tn} - E - i\Gamma_n)/R_y + \frac{\mu}{M_{\mathrm{tot}}}\left(\frac{x_{\frac{3}{2},N}}{R}\right)^2},$$

$$f_N = \frac{1}{6\pi}\left|j_2\left(x_{\frac{3}{2},N}\right)\right|^{-2} x_{\frac{3}{2},N}^2 \left[\int_0^1 u^3 du \prod_{s=1}^{\infty}\left(1 - \frac{x_{\frac{3}{2},N}^2}{x_{\frac{3}{2},s}^2}u^2\right)\right]^2, \qquad (5)$$

$$R = \frac{R_{\max}}{a^*},$$

$$f_{n1} = \frac{32(n^2-1)}{3n^5}\left[\frac{nr_0(r_0 + 2a^*)}{2r_0(r_0 + na^*)}\right]^6,$$

where $j_N(x)$ are the spherical Bessel functions $(N = 1, 2, \ldots)$, $x_{N,s}$ are roots of the equation $j_N(x) = 0$, $s = 1, 2, \ldots$, $a^* = 1.1$ nm is the Rydberg radius and E_{Tn} are energies of excitonic levels. The $r_0 = 1.1$ nm is the so-called coherence radius [41]. The damping coefficients of the excitonic levels Γ_n are taken from the Ref. [42] and include phonon interactions [43–45]. Their values are consistent with experimental results from Ref. [11].

The absorption coefficient α is calculated from [11]

$$\alpha(E) = \sum_{n=2}^{N} C_n \frac{\frac{\Gamma_n}{2} + 2q_n(E - E_n)}{\left(\frac{\Gamma_n}{2}\right)^2 + (E - E_n)^2}, \qquad (6)$$

where C_n is the amplitude that is proportional to the oscillator strength and q_n is the asymmetry parameter. The values of C_n are proportional to the area under the peaks of the imaginary part of susceptibility given by Eq. (5) and normalized to obtain an exact match the experimental value of α for $n = 2$. Due to the fact that the location of asymmetric peak depends on the

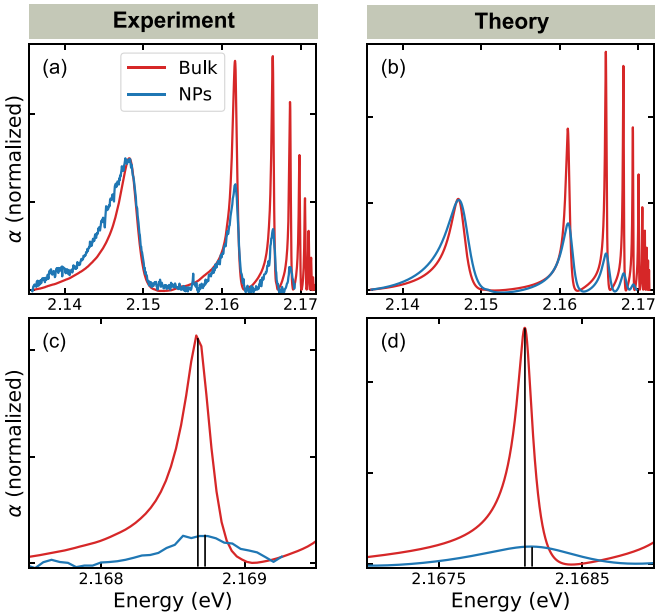

FIG. 4. (a, c) Experimental and (b, d) theoretical absorption spectra of bulk Cu_2O NPs in the full energy range and in the vicinity of $n = 5$ state.

parameter q_n, we used the initial values from Ref. [11] and adjusted them to fit to the measured peak locations.

Figure 4 shows a comparison of experimental and calculated absorption spectra with the phonon background subtracted. For background subtraction local minima between absorption peaks are found and connected by straight lines and everything below these lines is subtracted from the original spectra. The bulk crystal spectrum is also calculated from Eq. (5) by taking a very large NP radius $R > 10\,\mu$m. Due to the relatively large size of considered NPs and the corresponding confinement energy shifts on the order of $\sim 10\,\mu$eV, the direct observation of them can be challenging. To get a clearer picture of the results, the absorption coefficient obtained for bulk and nanoparticle systems has been normalized and the NP spectrum was shifted to obtain an exact match of $n = 2$ lines, removing the influence of different experimental conditions such as temperature mentioned before. In such a case, we observe a difference of $\Delta E \sim 25\,\mu$eV between bulk and NP lines for $n = 5$ state [vertical lines on Figs. 4(c) and 4(d)], both in the experimental spectra and calculation results. This amounts to the difference between the confinement energy of the $n = 5$ and $n = 2$ states, the latter one being negligible. This result is a close match to the theoretical predictions of Konzelmann *et al.* [23].

Our calculations show an excellent match between the measured oscillator strength and the theoretical estimates when the size distribution of the nanoparticles in considered [blue line in Fig. 3(a)]. The calculation for single NP size ($R = 350$ nm) fails to fully explain the oscillator strength reduction [orange line in Fig. 3(a)], further confirming that quantum dot size distribution is crucial to the understanding of the observed effects. Moreover, upper confinement states ($N > 1$) contribute to $\sim$23% of the peak area for $n = 5$, with a smaller effect for $n < 5$. The calculated linewidths match the experimental data for $n = 3, 4, 5$, while slightly underestimating the linewidth of $n = 2$ state [blue line in Fig. 3(b)]. Again, we find that it is crucial to take into account the size distribution of the NPs, further evidencing the effect of NP size.

V. DISCUSSION

Previous studies [11] showed that the power-dependent optical bleaching (reduction of peak area) only becomes visible for $n = 12$ for a pump intensity of ~ 1 mW/mm^2. Moreover, the intensity required to see optical bleaching scales as n^{10}. Therefore, to notice any nonlinearities at $n = 6$ one needs laser power on the order of 1 W/mm^2. The intensity of the illuminating light in our experiment (~ 1 mW/mm^2) is sufficiently low that the nonlinear effects observed in bulk can be neglected for the observed excitonic states. We note that in nanoparticles, the blockade diameter can become comparable to particle size for low n [46]. The intensities in our experiment, however, are three orders of magnitude weaker than that required to reach the blockade effect.

The reduction in oscillator strength due to damage to crystal structure can be ruled out since we observe this reduction in natural as well as synthetic NPs [47]. Strain on Cu_2O crystals can cause a change in the absorption strength due to change from isotropic to anisotropic np states [48]. The substrates can exert stress on Cu_2O crystals and affect the exciton transitions especially if the crystal is glued onto the cold finger or strongly sandwiched between two substrates. However, the nanoparticles here are held in place only by the van der Waals forces.

Electron-hole plasma generated due to the incident broadband light can affect the excitons. The collision of excitons with electron-hole plasma results in the reduction of exciton lifetime, broadening of the transitions as well as reducing the exciton oscillator strength. However, this effect was observed [49] to be significant only for n levels higher than $n = 10$.

The quantum confinement, however, is the dominant effect here. Theoretically, for $n = 5$ excitons in Cu_2O three dimensional confinement to $700\,\mu$m diameter, the lowest confinement state ($N = 1$) would exhibit a blueshift of $\sim 20\,\mu$eV [23], which is an order of magnitude smaller than the linewidth of the $n = 5$ transition. However, the states $N = 2, 3, 4, \ldots$ provide a nontrivial contribution to the total area of the observed excitonic line, which is a measure of oscillator strength. This is shown on the Fig. 5, where $N = 1, 2, 3$ states are marked by red, blue, and green lines, respectively. Since the energy shift of those states is proportional to N, it can reach values of over $200\,\mu$eV for $N > 2$. Moreover, for the given dot radius R, the energy shift is approximately proportional to R^{-2} and a relatively large energy shift on the order of 0.5 meV can be expected at the lower end of the obtained NP sizes. This is clearly seen in Fig. 5, where strongly blue-shifted peaks corresponding to small NPs are visible. All these factors contribute to the shape of the total line (black curve) and result in an apparent reduction of the oscillator strength; every observed excitonic line is an overlap of the primary confinement state ($N = 1$) and multiple blue-shifted higher states which are too close to each other to discern them on the spectrum. The contribution of these states is twofold.

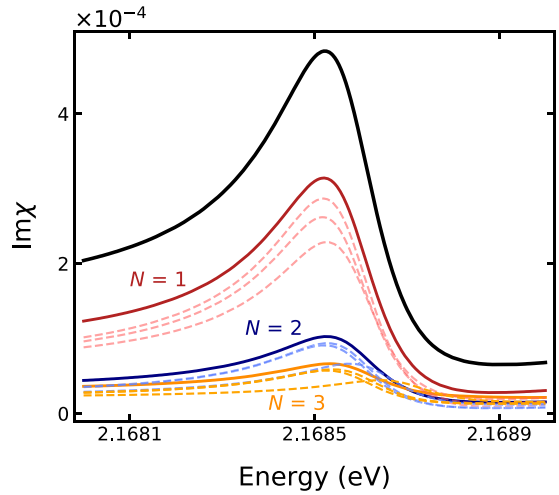

FIG. 5. Imaginary part of susceptibility calculated for $n = 5$ and various N values and dot sizes. For each N, a sample of three individual dot sizes is shown (dashed lines) along with an average (solid lines). The normalized sum over all confinement states and dot sizes is depicted as a black solid line.

(1) They make the transitions more symmetric. Since they have higher energy than the $N = 1$ state, their effect is more pronounced on the r.h.s. of the absorption peak; this is visible in Fig. 4(c) and 4(d) where the asymmetric lineshape of the bulk crystal is transformed into Gaussian shape. The effect is also visible for lower n states [Figs. 4(a) and 4(b)], but it is much less pronounced due to smaller energy shifts. (2) They significantly increase the background absorption. Since the oscillator strength of confinement states quickly decreases with N, their contribution affects mostly the base of the absorption line. The widened bases overlap, forming a strong absorptive background. This greatly reduces the area of the peak visible above that background resulting in an apparent reduction of the oscillator strengths.

In conclusion, we successfully observed Rydberg excitons in nanoparticles of Cu_2O. Through optical spectroscopy, we showed that reducing the size of the system leads to a subsequent reduction in the oscillator strength and an apparent linewidth broadening. We explained our observations through the quantum confinement of the excitons in the nanoparticles. Our work paves the way for exploiting Cu_2O Rydberg excitons in the nanoscale for their large nonlinearities.

The research data underpinning this publication can be accessed at [50].

ACKNOWLEDGMENTS

We acknowledge EPSRC Grant No. EP/S014403/1 and The Royal Society RGSR2192174. K.O. acknowledges EPSRC for Ph.D. studentship support through Grant No. EP/L015110/1. S.K.R. acknowledges the Carnegie Trust for Universities of Scotland Grant No. RIG009823. We thank Michael Huang, Matthew Jones, Stephen Lynch, Stefan Scheel, and Mikhail M. Glazov for fruitful discussions.

[1] R. W. Keyes, IBM J. Res. Dev. **32**, 84 (1988).
[2] D. D. Awschalom, L. C. Bassett, A. S. Dzurak, E. L. Hu, and J. R. Petta, Science **339**, 1174 (2013).
[3] M. H. Devoret and R. J. Schoelkopf, Science **339**, 1169 (2013).
[4] J. C. Loredo, N. A. Zakaria, N. Somaschi, C. Anton, L. de Santis, V. Giesz, T. Grange, M. A. Broome, O. Gazzano, G. Coppola, I. Sagnes, A. Lemaitre, A. Auffeves, P. Senellart, M. P. Almeida, and A. G. White, Optica **3**, 433 (2016).
[5] K. F. Mak and J. Shan, Nat. Photonics **10**, 216 (2016).
[6] M. F. Gonzalez-Zalba, arXiv:1801.06722 [cond-mat.mes-hall] (2018).
[7] M. Fox, *Optical Properties of Solids*, 2nd ed., Oxford master Series in Condensed Matter Physics Vol. 3 (Oxford University Press, Oxford, 2011).
[8] M. Hayashi and K. Katsuki, J. Phys. Soc. Jpn. **7**, 599 (1952).
[9] B. K. Meyer, A. Polity, D. Reppin, M. Becker, P. Hering, B. Kramm, P. J. Klar, T. Sander, C. Reindl, C. Heiliger, M. Heinemann, C. Müller, and C. Ronning, *Oxide Semiconductors*, edited by B. G. Svensson, S. J. Pearton, and C. Jagadish, Semiconductors and Semimetals, Vol. 88 (Elsevier, 2013), pp. 201–226.
[10] H. Matsumoto, K. Saito, M. Hasuo, S. Kono, and N. Nagasawa, Solid. Stat. Comm. **97**, 5 (1996).
[11] T. Kazimierczuk, D. Fröhlich, S. Scheel, H. Stolz, and M. Bayer, Nature **514**, 343 (2014).
[12] J. Thewes, J. Heckötter, T. Kazimierczuk, M. Aßmann, D. Fröhlich, M. Bayer, M. A. Semina, and M. M. Glazov, Phys. Rev. Lett. **115**, 027402 (2015).
[13] P. Grünwald, M. Aßmann, J. Heckötter, D. Fröhlich, M. Bayer, H. Stolz, and S. Scheel, Phys. Rev. Lett. **117**, 133003 (2016).
[14] J. Heckötter, M. Freitag, D. Fröhlich, M. Aßmann, M. Bayer, M. A. Semina, and M. M. Glazov, Phys. Rev. B **96**, 125142 (2017).
[15] J. Heckötter, M. Freitag, D. Fröhlich, M. Aßmann, M. Bayer, M. A. Semina, and M. M. Glazov, Phys. Rev. B **95**, 035210 (2017).
[16] M. Takahata and N. Naka, Phys. Rev. B **98**, 195205 (2018).
[17] S. O. Krüger and S. Scheel, Phys. Rev. B **97**, 205208 (2018).
[18] S. A. Lynch, C. Hodges, W. W. Langbein, L. Gallagher, J. Rogers, C. S. Adams, M. P. A. Jones, and R. P. Singh, in *2018 20th International Conference on Transparent Optical Networks (ICTON)* (IEEE, Bucharest, 2018), pp. 1–4.
[19] J. Mund, C. Uihlein, D. Fröhlich, D. R. Yakovlev, and M. Bayer, Phys. Rev. B **99**, 195204 (2019).
[20] S. Zielińska-Raczyńska, G. Czajkowski, K. Karpiński, and D. Ziemkiewicz, Phys. Rev. B **99**, 245206 (2019).
[21] M. P. A. Jones, L. G. Marcassa, and J. P. Shaffer, J. Phys. B: At., Mol. Opt. Phys. **50**, 060202 (2017).
[22] V. Walther, R. Johne, and T. Pohl, Nat. Commun. **9**, 1309 (2018).
[23] A. Konzelmann, B. Frank, and H. Giessen, J. Phys. B: At., Mol. Opt. Phys. **53**, 024001 (2020).
[24] N. Naka, S. Hashimoto, and T. Ishihara, Jpn. J. Appl. Phys. **44**, 5096 (2005).

[25] S. Steinhauer, M. A. M. Versteegh, S. Gyger, A. W. Elshaari, B. Kunert, A. Mysyrowicz, and V. Zwiller, Commun. Mater. **1**, 11 (2020).
[26] A. M. Smith and S. Nie, Acc. Chem. Res. **43**, 190 (2010).
[27] M. Khazali, K. Heshami, and C. Simon, J. Phys. B: At., Mol. Opt. Phys. **50**, 215301 (2017).
[28] S. Baur, D. Tiarks, G. Rempe, and S. Dürr, Phys. Rev. Lett. **112**, 073901 (2014).
[29] See Supplemental Material at http://link.aps.org/supplemental/10.1103/PhysRevB.103.245426 for setup.
[30] P. W. Baumeister, Phys. Rev. **121**, 359 (1961).
[31] A. Jolk and C. F. Klingshirn, physica status solidi (b) **206**, 841 (1998).
[32] Y. Toyozawa, J. Phys. Chem. Solids **25**, 59 (1964).
[33] V. T. Agekyan, B. S. Monozon, and I. P. Shiryapov, physica status solidi (b) **66**, 359 (1974).
[34] See Supplemental Material at http://link.aps.org/supplemental/10.1103/PhysRevB.103.245426 for synthetic nanoparticles spectra.
[35] K. P. O'Donnell and X. Chen, Appl. Phys. Lett. **58**, 2924 (1991).
[36] See Supplemental Material at http://link.aps.org/supplemental/10.1103/PhysRevB.103.245426 for temperature dependence.
[37] A. I. Ekimov, A. A. Onushchenko, A. G. Plyukhin, and A. L. Efros, Zh. Eksp. Teor. Fiz. **88**, 1490 (1985).
[38] A. I. Ekimov, A. A. Onushchenko, M. E. Raikh, and A. L. Efros, Zh. Eksp. Teor. Fiz. **90**, 1795 (1986).
[39] D. Ziemkiewicz, K. Karpiński, G. Czajkowski, and S. Zielińska-Raczyńska, Phys. Rev. B **101**, 205202 (2020).
[40] See Supplemental Material at http://link.aps.org/supplemental/10.1103/PhysRevB.103.245426 for calculation of quantum dot susceptibility.
[41] S. Zielińska-Raczyńska, G. Czajkowski, and D. Ziemkiewicz, Phys. Rev. B **93**, 075206 (2016).
[42] D. Ziemkiewicz and S. Zielińska-Raczyńska, Opt. Express **27**, 16983 (2019).
[43] H. Stolz, F. Schöne, and D. Semkat, New J. Phys. **20**, 023019 (2018).
[44] H. Zhao, S. Wachter, and H. Kalt, Phys. Rev. B **66**, 085337 (2002).
[45] S. Rudin and T. L. Reinecke, Phys. Rev. B **41**, 3017 (1990).
[46] See Supplemental Material at http://link.aps.org/supplemental/10.1103/PhysRevB.103.245426 for blockade diameter.
[47] See Supplemental Material at http://link.aps.org/supplemental/10.1103/PhysRevB.103.245426 for synthetic nanoparticles spectra.
[48] V. T. Agekyan, physica status solidi (a) **43**, 11 (1977).
[49] J. Heckötter, M. Freitag, D. Fröhlich, M. Aßmann, M. Bayer, P. Grünwald, F. Schöne, D. Semkat, H. Stolz, and S. Scheel, Phys. Rev. Lett. **121**, 097401 (2018).
[50] https://doi.org/10.17630/633aa0f8-bf54-43e4-ad11-417ef94549d9.